Letters

Operating Frequency Prediction of Piezoelectric DC–DC Converters

Lucas de Araujo Pereira, *Student Member, IEEE*, Adrien Morel, *Member, IEEE*, Mustapha Touhami, *Member, IEEE*, Théo Lamorelle, Ghislain Despesse, and Gaël Pillonnet, *Senior Member, IEEE*

***Abstract*—Piezoelectric dc–dc converters operate between the series and parallel frequencies of the piezoelectric resonator to achieve soft switching and energy-balance conditions. This letter presents an experimentally validated model to accurately predict the operating frequency, the switching angles, and the piezoelectric current for any six-phase piezoelectric dc–dc converter. This model reduces the transient simulation's calculation time to reach the steady state. It can be used to initially setup the switching angles in the experiment or to predict the high-frequency spectrum generated by the converter cycle.**

***Index Terms*—DC–DC converter, mathematical model, operating frequency, piezoelectric resonator (PR).**

I. Introduction

Wide bandgap adoption among switching devices enables a drastic increase of the switching frequency in order to reduce the power converter size. However, the gain from high-frequency operation is mainly limited by the magnetic components' performances that scale sublinearly with frequency [1]. In order to overcome the scaling limitations imposed by inductors, an emerging topology based on piezoelectric electromechanical resonators (PR) has been recently introduced in [2], then extended in [3]. As shown in Fig. 1(a), the PR dc–dc converter (PRC) is composed of arrangements of switching devices that allow adiabatic energy transfers through a dc-blocking PR. Promising experimental results show 10s W/cm^3 power density while maintaining high efficiency ($> 95\%$) at relatively low frequency ($\sim$100 kHz) [2], [3]. Pollet *et al.* [2] and Touhami *et al.* [4] have already associated a self-tracking feedback to control each phase for sub-MHz operating range. Touhami *et al.* [4] and Braun *et al.* [5] have also proven the performance of the PR in MHz range, showing the capability to scale down with frequency. Braun *et al.* [5] and Boles *et al.* [10] point out the main performance criteria of PRCs: high electromechanical coupling and high mechanical quality factors. The mentioned challenges are mainly the control of switching instants at high frequency [4] and the reduction of spurious resonant modes [2], [5]. To help the designer to explore the PRC performance, an accurate prediction of switching cycle timing at early design stages is required.

In opposite to the conventional converter structures, the cycle period of PRCs is fixed by the PR dynamics and electrical conditions. As shown in previous articles, the operating frequency (f) varies from series (f_s) to parallel (f_p) resonances PR frequencies (f_p /f_s < 1.3), mainly dictated by the coupling factor [5]. The aforementioned articles make strong assumptions regarding the cycle period value to analytically approximate the converter's characteristics, such as the power efficiency or the piezoelectric current magnitude with tractable expressions. However, the precise cycle period enables to carefully size the PR, to accurately evaluate the piezoelectric current magnitude over a full power range, and to quantify the high-frequency spectrum in order to avoid that some harmonics excite the higher PR resonance modes.

Based on a modeling approach adopted by the piezoelectric energy harvesting community for strong coupling PR [6], [7], this letter proposes to model the impact of the energy transfers (imposed by the converter topology) on the PR dynamics by adding an electrically induced capacitor C_e and negative resistor R_e [see Fig. 1(b)]. Thanks to the well-known first harmonic approximation (FHA) [6] and the van Dyke PR model (input capacitance C_p in parallel with an *RLC* branch) [8], [9], this letter introduces a merged model combining the PR dynamics and the electrically induced stiffness linked to the voltage across the PR, which is imposed by the PRC operation [see Fig. 1(c)]. The coefficient α in the proposed merged model is derived from the frequency-spectrum decomposition of the piezoelectric voltage v_p mixed with the PR impedance.

This letter describes how to calculate the coefficient α, the PR current amplitude I_m, and the switching angles x_i [3] for any six-phase PRC topologies. This method is applied to various PRC topologies used in previous articles [2], [4], [5] and proves that the proposed model is in good agreement with the experimental results. Other benefits of this modeling are also discussed, e.g., reaching the steady state faster and evaluating spurious modes effect.

Manuscript received July 27, 2021; revised September 7, 2021; accepted September 17, 2021. Date of publication September 24, 2021; date of current version November 30, 2021. *(Corresponding author: Lucas de Araujo Pereira.)*

The authors are with DRT, CEA-Leti, 38054 Grenoble, France (e-mail: lucas-henrique.dearaujopereira@cea.fr; adrien.morel@univ-smb.fr; mustapha.touhami@cea.fr; theo.lamorelle@cea.fr; ghislain.despesse@cea.fr; gael.pillonnet@cea.fr).

Color versions of one or more figures in this article are available at https://doi.org/10.1109/TPEL.2021.3115182.

Digital Object Identifier 10.1109/TPEL.2021.3115182

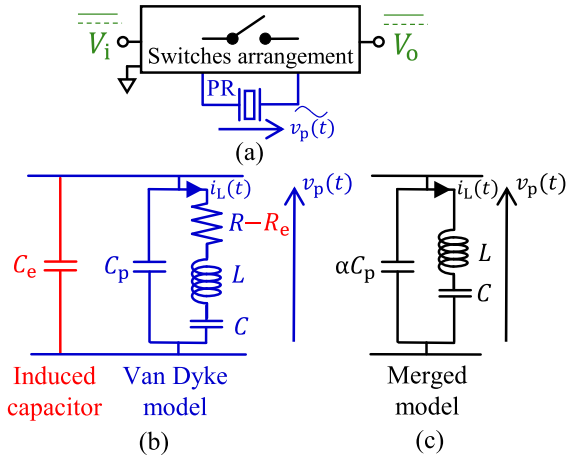

Fig. 1. (a) PRC. (b) Electrically induced capacitor. (c) Merged model.

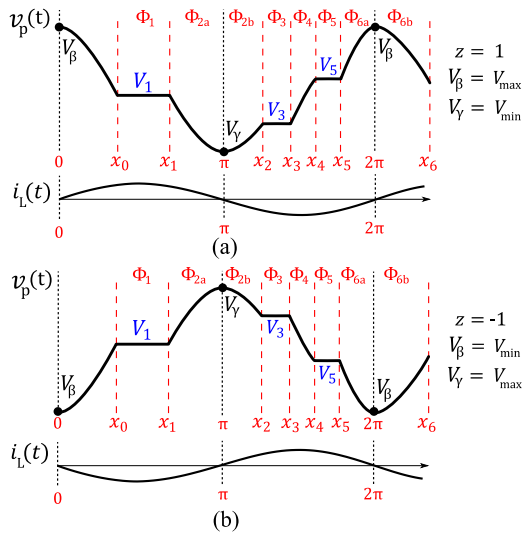

Fig. 2. (a) Generic form of $v_p(t)$ and $i_L(t)$ of a six-phase cycle with $z = 1$. (b) Generic form of $v_p(t)$ and $i_L(t)$ of a six-phase cycle with $z = -1$.

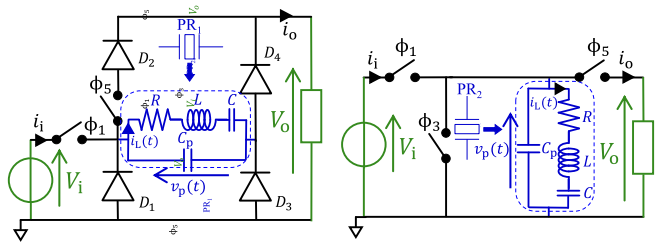

Fig. 3. PRC topologies used during the experimental model validation.

II. Method Description

A. Operating Principle and Notations

The PRC operating principle is well described in [2]–[5]. To summarize and introduce the model's notations, this letter reminds some notions in Section II-A. The PRC is based on controlling the switching cycle (see Fig. 2) synchronized with the PR oscillation by applying *constant voltage phases* (CVP) alternating with *constant charge phases* (CCP), while ensuring both charges and energy balance [2], [3].

1) CVP: PR is connected to combinations of input, output, and ground voltages, allowing the energy exchange between PR and voltage sources.
2) CCP: PR is open circuited, allowing a variation of the PR voltage $v_p(t)$ up to the value of the next CVP, enabling the soft switching of the PRC.

A six-phase cycle switching sequence is determined as follows:

1) three different CVP by cycle (V_1, V_3, and V_5), where V_3 and V_5 are located in the second half of the PR vibration period ($\forall x_i \in [\pi, 2\pi]$);
2) three different CCP by cycle (v_2, v_4, and v_6);
3) at least one phase that is connected to each of the input voltage V_i and output voltage V_o;
4) the voltages V_1, V_3, and V_5 can be equal to any linear combination of $\pm V_i$, $\pm V_o$, and 0.

For model genericity, the switching sequence is classified into two cases, as depicted in Fig. 2, where $V_{\max}$ and $V_{\min}$ are, respectively, the maximum and the minimum voltage values reached by $v_p(t)$. The coefficient z represents the initial phase of $i_L(t)$. Some sequences are given as an example in Table I (K and μ_i are explained subsequently).

The switching sequence notation here is different from the article presented in [3]. The phase reference on the waveform $i_L(t)$ is chosen [see either Fig. 2(a) or Fig. 2(b)] in order to locate V_3 and V_5 in the second half of the PR vibration period ($\forall x_i \in [\pi, 2\pi]$). This phase reference is necessary for the model genericity for any six-phase PRC topology.

TABLE I
Switching Sequences' Parameters' Examples

ref	*Switching sequence*			*Voltage conversion*	z	μ_1	μ_3	μ_5	*K*
	V_1	V_3	V_5						
[2]	V_i	0	V_o	$V_i < V_o$	1	0	0	1	$\frac{V_i}{2V_o}$
	V_o	V_i	0	$V_i > V_o$	-1	1	0	0	½
[3]	V_o	$V_i - V_o$	0	$V_i > 2V_o$	-1	1	1	0	$\frac{V_i}{2(V_i - V_o)}$
	$V_i - V_o$	0	V_o	$2V_o > V_i > V_o$	1	1	0	1	$\frac{V_i}{2V_o}$
[4]	V_o	$V_i - V_o$	$-V_o$	$0.5V_i > V_o$	-1	1	1	1	1
[5]	0	$V_i - V_o$	$-V_o$	$V_i > V_o$	-1	0	1	1	½

B. Piezoelectric Current Amplitude

The PR current i_L is assumed to be purely sinusoidal with an amplitude I_m given by (1) for any switching sequence

$$I_m = \pi \left(\frac{P_{\text{out}}}{2KV_o} + fC_p \left(V_{\max} - V_{\min} \right) \right) \tag{1}$$

where P_{out} is the transferred power, f is the operating frequency, and K is the charge utilization factor inspired in [3]. K can be calculated as the ratio between the CVP connected to the output and all the CVP

$$K = \frac{\mu_1 \left(V_3 - V_5 \right) + \mu_3 \left(V_1 - V_5 \right) + \mu_5 \left(V_3 - V_1 \right)}{2 \left(V_3 - V_5 \right)} \tag{2}$$

where μ_i is equal to 1, when the *i*th phase is connected to the output and 0 otherwise (see Table I).

C. Switching Angles

The six switching angles have to be carefully fixed to allow soft switching operation, except x_3 (or x_4), which is the degree of freedom of the period that must be adjusted to achieve the desired P_{out} and V_o. From the general waveform, as given in Fig. 2, the duration of each phase is calculated relatively to the cycle period using the following equations:

$$x_0 = \cos^{-1}\left(1 + z\frac{(V_1 - V_\beta)}{A}\right) \tag{3}$$

$$x_1 = \cos^{-1}\left(-1 - z\frac{(V_\gamma - V_1)}{A}\right) \tag{4}$$

$$x_2 = \cos^{-1}\left(-1 + z\frac{(V_3 - V_\gamma)}{A}\right) \tag{5}$$

$$x_3 = 2\pi - \cos^{-1}\left(\frac{\theta_2 V_3 + V_5\left(z\frac{V_5 - V_3}{A} - \theta_5\right) - V_1(\theta_1 - \theta_0) + z(\pi R I_m)}{(V_3 - V_5)}\right) \tag{6}$$

$$x_4 = 2\pi - \cos^{-1}\left(\theta_3 + z\frac{(V_5 - V_3)}{A}\right) \tag{7}$$

$$x_5 = 2\pi - \cos^{-1}\left(1 - z\frac{(V_\beta - V_5)}{A}\right) \tag{8}$$

$$x_6 = 2\pi + x_0 \tag{9}$$

where $A = I_m/(2\pi f C_p)$ and $\theta_i = \cos(x_i)$.

D. Fundamental of the Voltage Across PR

If the operating frequency f is assumed to be constant (equal to f_s or f_p as in [2] and [3]), I_m and x_i can be analytically derived from (1) to (9). However, f varies between f_s and f_p, inducing non-negligible errors. In practice, the operating frequency is found by adjusting manually the frequency and the switching angles until finding the zero voltage switching (ZVS) operation as in [2] or by introducing self-synchronization blocks as in [3]. To calculate I_m and x_i precisely without any adjustment, this letter proposes the following method.

Considering that the PR exhibits a large quality factor and operates in the steady state, the FHA method is applied in order to evaluate the impact of the fundamental harmonic of the piezoelectric voltage on the PR dynamics [6], [7]. The fundamental of the piezoelectric voltage $v_p(t)$ can be expressed as

$$v_p(t)\,|_{n=1} = a_1\,\cos(2\pi f t) + b_1 \sin(2\pi f t) \tag{10}$$

where a_1 and b_1 are the firsts Fourier coefficients. Physically, they can be associated with an electrically induced stiffness (modifying the PR resonance frequency) and an electrically induced damping as identified later in (17) and (18). We can calculate these coefficients for any six-phase PRC

$$a_1 = \sum_{k=0}^{2}\left\{z\frac{V_{k+1}}{\pi}(\sin x_{2k+2} - \sin x_{2k}) + \frac{I_m}{2\pi^2 f C_P} \times \left[\frac{x_{2k+2} - x_{2k+1}}{2} + \frac{\sin 2x_{2k+2} - \sin 2x_{2k+1}}{4} - \cos x_{2k+1}(\sin x_{2k+2} - \sin x_{2k+1})\right]\right\} \tag{11}$$

$$b_1 = \sum_{k=0}^{2}\left\{z\frac{V_{k+1}}{\pi}(\cos x_{2k} - \cos x_{2k+2}) + \frac{I_m}{\pi\omega C_P} \times \left[\frac{\cos 2x_{2k+1} - \cos 2x_{2k+2}}{4} - \cos x_{2k+1}(\sin x_{2k+1} - \sin x_{2k+2})\right]\right\} \tag{12}$$

where x_i are the switching angles calculated with (3)–(9) and V_k is the CVP (V_1, V_3, and V_5).

E. Merged Model

By applying mesh analysis to the PR equivalent van Dyke model [see Fig. 1(b)], (10) can be derived as

$$v_p(t) = L\frac{dq^2}{d^2t} + R\frac{dq}{dt} + \frac{1}{C}q. \tag{13}$$

Since the current $i_L(t)$ and electric charge q are linked by (14), the expression of the charge is given by (15)

$$i_L\ (t) = I_m\ \sin(2\pi f t) = \frac{dq}{dt} \tag{14}$$

$$q\ =\ -\frac{I_m}{2\pi f}\cos(2\pi f t)\,. \tag{15}$$

Based on the FHA, (10) can be combined with (13)–(15) to obtain the second-order differential equation governing the charge transfer into the PR

$$L\frac{d^2q}{dt^2} + \left(R - \frac{b_1}{I_m}\right)\frac{dq}{dt} + \left(\frac{1}{C} + \frac{a_1 2\pi f}{I_m}\right)q\ =\ 0. \tag{16}$$

Equation (16) can be identified as an *RLC* branch [see Fig. 1(b)], including the PR van Dyke model along with electrically induced components (C_e and R_e) due to the switching sequence at first harmonic. The electrically induced capacitor C_e and resistor R_e are deduced by

$$C_e = \frac{I_m}{a_1 2\pi f} \tag{17}$$

$$R_e = \frac{b_1}{I_m}. \tag{18}$$

In steady-state operation, the PR is energy balanced over a complete switching sequence; thus, the electrically induced resistor compensates the PR losses introduced by R

$$R_e = \frac{b_1}{I_m}\ =\ -R. \tag{19}$$

The averaged behavior over one cycle given by (16) can be represented as a merged model [see Fig. 1(c)] by merging C_e

TABLE II
PARAMETERS OF THE PR USED DURING THE VALIDATION

PR	L	C	C_p	R	f_s	Q	k
PR_1	1.1 mH	2.9 nF	8.4 nF	0.4 Ω	89 kHz	1537	52%
PR_2				0.6 Ω		1025	

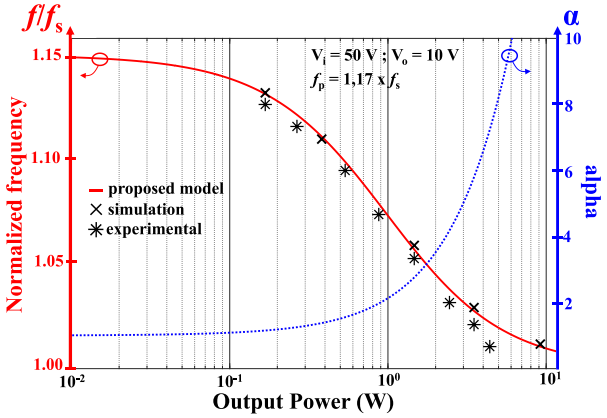

Fig. 4. Operating frequency versus the output power for sequence used in [4].

into C_p using the coefficient α (20)

$$\alpha = \frac{I_m}{a_1 2\pi f C_p}. \tag{20}$$

For the sinusoidal steady state, the resonance frequency of the merged model can be obtained by solving (21)

$$\left(4\pi^2 LC\right) f^2 + \left(2\pi \frac{I_m}{a_1}\right) f - 1 = 0. \tag{21}$$

The previous equations form a system

$$\begin{cases} (1-2) \\ (3-9) \\ (11) \\ (21) \end{cases} \leftrightarrow \begin{cases} I_m = F\left(f, P_{\text{out}}\right) \\ x_i = G\left(I_m, v_p\right) \\ a_1 = H\left(x_i,\ I_m, f, v_p\right) \\ f = J\left(a_1, I_m\right) \end{cases}. \tag{22}$$

The system (22) is not analytically solvable. Therefore, this system is numerically solved in order to find the operating frequency, the current amplitude I_m, and x_i.

III. Experimental Validation

Two PRC topologies showed in Fig. 3 have been chosen to compare the proposed model to transient simulations and experimental results. The constant voltages V_1, V_3, and V_5 are given in Table I, for the step-down [4] and step-up [2] topologies, respectively. The PRC experimental setup is described in these two articles [2], [4], and the $PR_{1,2}$ parameters are given in Table II.

Figs. 4 and 5 show, from experimental data, SPICE simulations, and the numerical solved system given by (22), the variation of the operating frequency (normalized by f_s) and coefficient α as a function of the output power for the two topologies ([4] and [2]). The model prediction matches the electrical simulations, i.e., $\Delta f_{\max} = 10$ Hz, equivalent to 0.07% error on $[f_p - f_s]$. It gives a reasonable accuracy, i.e., $< 1.5\%$ error compared with the experimental results.

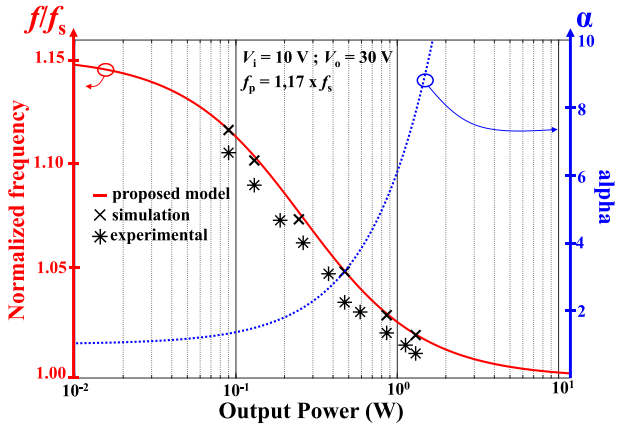

Fig. 5. Operating frequency versus the output power for sequence used in [2].

A small deviation between the experimental curve and the theoretical and simulation curves is observed in Fig. 5 due to an additional parasitic PR connection. For low power transfer, α tends to 1, meaning no capacitance is induced by the converter ($C_e \approx 0$), and the PR operates at its open-circuit resonance frequency ($f = f_p$). For high output power, α tends to infinity ($C_e \to +\infty$) as the converter cycle induces additional stiffness on PR, thus reducing the operating frequency.

IV. Discussions

A. Faster Steady-State Convergence

To design an optimal PRC (e.g., sizing the switches or choosing a particular PR), several electrical simulations are needed. Reaching the steady state faster is a key enabler to perform sweep simulations. The first method is to calculate the angles assuming a constant frequency ($f = f_s$), the targeted powers are not guaranteed, and the PRC operates without ZVS. The second method is to numerically sweep the frequency between f_p and f_s to find the right angles, derived from (3) to (9), to reach soft switching and the targeted output power. Considering a 10 Hz frequency step (same accuracy as the proposed model), 1500 electrical simulations are required (1 h of processing on a personal computer). Otherwise, this letter presents a third method that consists in determining the operating frequency and the angles x_i by calculation before running a single transient simulation (2.4 s of processing on a personal computer). Note that Boles *et al.* [3] propose an alternative numerical method to find the frequency based on solving differential equations, but the authors have not enough details to include this method in this comparison.

Fig. 6 illustrates the efficiency over a range of output power for the three aforementioned methods. Anew, the proposed model is still validated to give fast and accurate results to reach the steady state. The precalculated initial conditions from the proposed model can also be used during experimentation in order to set the angles x_i, thus reducing the losses before reaching the effective steady state.

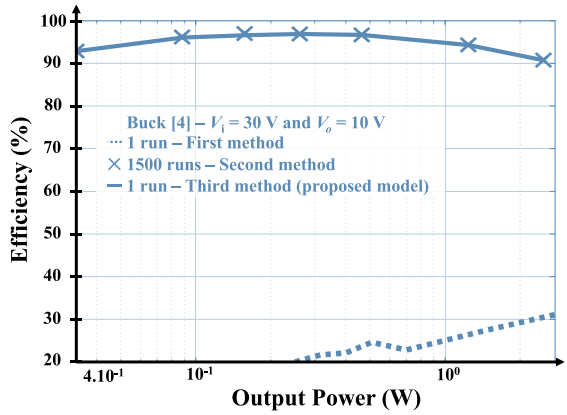

Fig. 6. Efficiency versus the output power based on sequence [2].

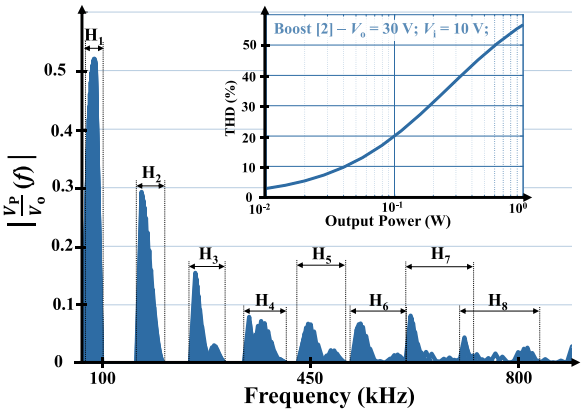

Fig. 7. Cumulative frequency spectrum from 0.01 to 1 W output power and THD based on sequence [2] over output power.

B. Spurious Mode Prediction

Pollet *et al.* [2] report an efficiency drop-off due to higher resonant modes excitation ($>f_p$). To predict this issue at an early design stage, the other Fourier coefficients ($a_i, b_i, i > 1$) can also be derived to predict the amplitude of the higher harmonics of v_p. Fig. 7 depicts the cumulative frequency spectrum and the total harmonic distortion (THD) across various output powers for the topology [2]. The proposed model predicts the frequencies and amplitude outside $[f_s, f_p]$, then can be combined with PR impedance measurements in order to evaluate the effect of spurious modes.

Braun *et al.* [5] also reported the non-negligible effect of other resonance modes on the efficiency of PRC, especially those located between f_s and f_p. If the PR impedance is known at an early design stage, the accurate frequency prediction allowed by the proposed model can also be used to predict the limitations on the output power. In [5], when the switching sequence ($V_i - V_o$, 0, V_o) is tested with a voltage conversion from $V_i = 50$ V to $V_o = 25$ V, the minimum measured power output is equal to 18 W. Above this operating frequency (6.82 MHz), the unwanted vibration modes cause the efficiency to drop. Based on the proposed model and using the data provided in [5], 15.5 W is the minimum power output value in order not to excite higher resonance modes (which is relatively close to the 18 W reported in [5]). It is still a way to validate the proposed model and underline its genericity for any six-phase PRC sequences.

V. Conclusion

This letter proposed a model to predict the operating frequency and switching angles accurately for any six-phase PRC topology. The proposed model is based on an electrically induced capacitor to emulate the effect of the switching sequence of PRC. The model has been experimentally validated. The model can be used to reduce the calculation time for transient simulations or to quickly reach ZVS operation by setting the right steady state. The model is also valuable for predicting the high-frequency spectrum generated by PRC on PR and to evaluate the excitation of the PR higher resonance modes.

References

[1] C. R. Sullivan, B. A. Reese, A. L. F. Stein, and P. A. Kyaw, "On size and magnetics: Why small efficient power inductors are rare," in *Proc. Int. Symp. 3D Power Electron. Integration Manuf.*, 2016, pp. 1–23.

[2] B. Pollet, G. Despesse, and F. Costa, "A new non-isolated low-power inductorless piezoelectric DC–DC converter," *IEEE Trans. Power Electron.*, vol. 34, no. 11, pp. 11002–11013, Nov. 2019.

[3] J. D. Boles, J. J. Piel, and D. J. Perreault, "Enumeration and analysis of DC–DC converter implementations based on piezoelectric resonators," *IEEE Trans. Power Electron.*, vol. 36, no. 1, pp. 129–145, Jan. 2021.

[4] M. Touhami, G. Despesse, and F. Costa, "A new topology of DC-DC converter based on piezoelectric resonator," in *Proc. IEEE 21st Workshop Control Model. Power Electron.*, 2020, pp. 1–7.

[5] W. D. Braun *et al.*, "Optimized resonators for piezoelectric power conversion," *IEEE Open J. Power Electron.*, vol. 2, pp. 212–224, Mar. 2021.

[6] A. Morel, G. Pillonnet, P. Gasnier, E. Lefeuvre, and A. Badel, "Frequency tuning of piezoelectric energy harvesters thanks to a short-circuit synchronous electric charge extraction," *Smart Mater. Struct.*, vol. 28, no. 2, 2018, Art. no. 025009.

[7] J. Liang and W.-H. Liao, "Impedance modeling and analysis for piezoelectric energy harvesting systems," *IEEE/ASME Trans. Mechatronics*, vol. 17, no. 6, pp. 1145–1157, Dec. 2012.

[8] K. S. van Dyke, "The piezo-electric resonator and its equivalent network," *Proc. Inst. Radio Eng.*, vol. 16, no. 6, pp. 742–764, Jun. 1928.

[9] G. Ivensky, I. Zafrany, and S. Ben-Yaako, "Generic operational characteristics of piezoelectric transformers," *IEEE Trans. Power Electron.*, vol. 17, no. 6, pp. 1049–1057, Nov. 2002.

[10] J. D. Boles, P. L. Acosta, Y. K. Ramadass, J. H. Lang, and D. J. Perreault, "Evaluating piezoelectric materials for power conversion," in *Proc. IEEE 21st Workshop Control Model. Power Electron.*, 2020, pp. 1–8.